

Contoured Bode Plot based Robust Decentralised Controller for Three-Input Integrated Dc-Dc Converter

M. MANOGNA, B. AMARENDRA REDDY, KOTTALA PADMA

Department of Electrical Engineering,
Andhra University College of Engineering,
Visakhapatnam, Andhra Pradesh,
INDIA

Abstract: - Designing controllers for multi-input multi-output (MIMO) integrated Dc-Dc converter is complicated due to shared elements, integrated structure, and relation between the input and output variables of the converter. In this work, a robust PID controller based on a Contoured Robust Controller Bode Plot (CRCBP) is designed for control of the three-input integrated Dc-Dc (TIID) converter. This method combines robust control with classical loop-shaping. In this procedure, the outlines of the robust metric are drawn on the Bode charts of the controller, and the controller is adjusted till its frequency response does not cross the contours of the robust metric to meet the stability and performance goals. The TIID converter is modeled using state-space analysis and a Transfer Function Matrix (TFM) is acquired from the small signal continuous time model. The interactions between the inputs and outputs of the converter are quantified and input-output pairing is identified by Relative Gain Array (RGA). The input-output pairing suggested by RGA decides the controller structure. Further, the weight functions (loop-shaping filters) are designed based on the TFM which represents the desired robustness and performance of the controller. These weight functions are used to define the robust metric for the controller design. Based on this, the CRCBP controller is designed iteratively. A standard TIID converter of power rating 288 W with input voltage levels of 24V, 30V, and 36V is considered to show the effectiveness of the proposed controller under varying operating conditions. The real-time simulation results disclose the proposed controller's superiority over the existing approaches in the literature.

Key-Words: - Hybrid Electric Cars, Renewable Energy Systems, Contoured Robust Controller Bode Plot (CRCBP), Three-Input Integrated Dc-Dc (TIID) converter, state-space modeling, small-signal analysis, Transfer Function Matrix (TFM), multivariable PID controller.

Received: April 22, 2024. Revised: October 25, 2024. Accepted: November 11, 2024. Published: December 16, 2024.

1 Introduction

It has been demonstrated that switched-mode MIMO converters are more adaptable, affordable, dependable, and efficient than single-input single-output (SISO) converters, [1], [2] and [3]. MIMO converters are used in the design of power electronic applications such as hybrid electric cars, [4], locomotives, and other systems, [5], powered by renewable energy sources, [6], [7]. Therefore, building multi-variable PID controllers for MIMO converters is more complex than for SISOs because of the integrated structure, shared components, and interactions between the input and output variables of the converter. With just three tuning parameters and a multitude of accessible methods, designing a SISO PID is quite easy, [8]. However, compared to a SISO scenario, the MIMO system has a significantly higher number of variables due to an increase in the process's control inputs and outputs. This makes the problem more difficult to solve.

Numerous studies have also been conducted on MIMO PID controllers. Even though PIDs make up over 90% of the controllers used in the market, MIMO PID controller design still has a lot of issues. Therefore, to construct MIMO PID controllers with improved performance, effective tuning techniques must be developed.

The recent research reports on many approaches to constructing resilient MIMO PID controllers for MIMO systems. For a two-input dc-dc converter system, a decentralized controller is designed using the effective transfer function method, [9], while a centralized controller is created using the equivalent transfer function methodology, [10]. For the two-input Buck-SEPIC dc-dc converter system, diagonal controllers are recommended using individual channel design (ICAD), [11]. A decoupler network is designed for a three-port dc-dc converter suitable for a satellite application to minimize control-loop interactions,

[12]. An interaction independent robust controller for a two-input fourth-order integrated (TIFOI) dc-dc converter is designed using the Loop Shaping design approach, [13]. Even if there are several methods for developing a TIID converter's controller, they nonetheless have drawbacks like:

- (i) Equivalent and effective transfer function methodologies require SOPDT models, [14],
- (ii) ICAD needs an initial controller, [15],
- (iii) H_∞ loop shaping design procedure requires uncertainty representation in co-prime factor form, [16], [17]
- (iv) Design of a suitable decoupling network is a tedious process, [18].

To address these limitations, the CRCBP method is implemented in [19]. This approach combines robust control with classical loop-shaping, [20], [21]. Using this procedure, the outlines of the robust metric are drawn on the Bode charts of the controller. The controller is adjusted till its frequency response does not cross the contours of the Robust Performance Metric (RPM) to meet the stability and performance goals.

Novelty of the work:

The CRCBP approach provides a novel controller design method that permits finite structured uncertainty and is based on the simple H_∞ - norm, without raising the amount of complexity in the design process, [19]. The available literature only provides controller design for single-input and dual-input dc-dc converters, [19], [21]. This paper attempts to implement CRCBP based multivariable controller for TIID converter. The detailed iterative controller design process is explained along with forbidden regions of RPM contours. At each stage of the iterative process, the relation between contoured plots and sensitivity plots is graphically shown. All the PI controllers in the iteration process that satisfy and violate RPM criteria and their relation with sensitivity function are explained graphically.

Contribution of the paper:

The following contributions are made from this work:

- (i) A fourth-order TIID converter is proposed in [22]. Here, the guidelines from [23], are applied to merge two boost converters with a buck-boost converter. The converter operation and dynamics are represented by a mathematical model. State space analysis

along with the small-signal averaging method is performed in each mode of operation to obtain the TFM.

- (ii) To determine the controller structure, interaction analysis is carried out to determine the converter's input-output pairing. Further, CRCBP based multi-variable controller is proposed for the TIID converter, which is a major contribution of the present work.
- (iii) Different operating situations, such as fluctuating source voltages, loads, or both, are simulated in real time, and the effects of parameter alterations on the dynamics of the converter system are examined.

Following this, the paper is organized as follows: Section 2 describes the mathematical modeling of the TIID converter and derivation of the TFM of the converter. Sections 3 and 4 depict the procedure for designing CRCBP controller and its implementation to control the TIID converter. Further, the real-time simulation results are disclosed in Section 5. Finally, the results drawn are shown as conclusions in Section 6.

2 Mathematical Modelling of TIID Converter

Based on the knowledge provided in [21], two boost converters as well as a buck-boost converter are combined in this study. Figure 1 depicts a traditional fourth-order TIID converter. Three separate input voltage sources V_{g1} , V_{g2} and V_{g3} are suggested for this integrated converter: and. In addition to controlling the output voltage V_o , Low Voltage Source (LVS) currents i_{g1} and i_{g2} are also controlled to ensure appropriate load distribution and uninterrupted power supply. The three switches on the TIID converter are each individually controlled by the relevant duty ratios d_1 , d_2 and d_3 . As a result, power can flow to the load from three separate sources either concurrently or individually, and the duty ratios serve as the converter's controlling inputs. As a result, TIID operates in four separate modes, as seen in Figure 2.

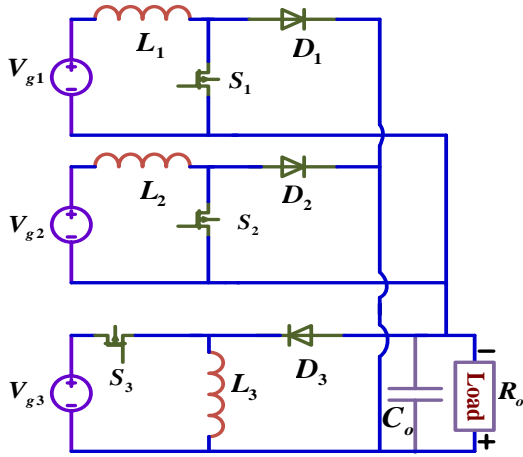


Fig. 1: Schematic of the TIID converter

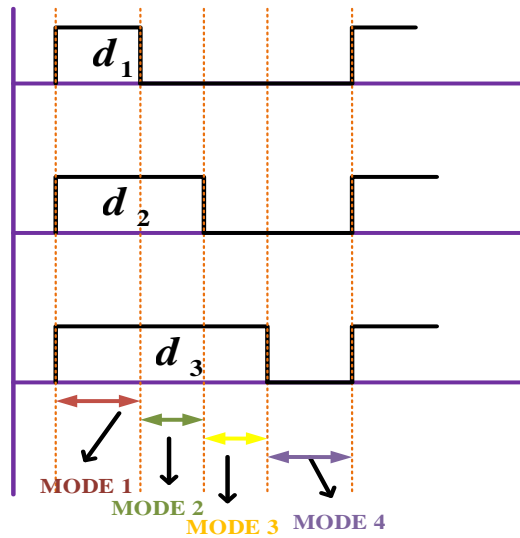


Fig. 2: TIID converter gating signals

This paper uses state space equations in each mode to analyze the converter dynamics and operations. As a result, a collection of transfer functions put together in TFM form serves as a model for the functional dependency between output and input variables. In all operating modes, the state-variable model and small-signal modeling are used to obtain the TFM.

Equations (1) and (2) provide the state-space equations for the four operating modes, where $i = 1, 2, 3, 4$. By averaging these state equations as

shown in (3) and applying a small change \hat{k} in each of the state variables as in (4), the small-signal modeling of the converter can be obtained, from there the TFM as given in (5) is developed in MATLAB environment. The detailed and complete derivation aspects of small-signal modeling of the TIID converter are given in [22].

$$\dot{x} = A_i x + B_i u, \quad y = E_{0i} x + F_{0i} u \quad (1)$$

$$y = \begin{bmatrix} v_0 \\ i_{g1} \\ i_{g2} \end{bmatrix} E_{0i} = \begin{bmatrix} E_1 \\ P_{1i} \\ P_{2i} \end{bmatrix} F_{0i} = \begin{bmatrix} F_1 \\ F_{1i} \\ F_{2i} \end{bmatrix} \quad (2)$$

$$\begin{bmatrix} A \\ B \\ E \\ F \end{bmatrix} = \begin{bmatrix} d_1 A_1 + (d_2 - d_1) A_2 + (d_3 - d_2) A_3 + (1 - d_3) A_4 \\ d_1 B_1 + (d_2 - d_1) B_2 + (d_3 - d_2) B_3 + (1 - d_3) B_4 \\ d_1 E_1 + (d_2 - d_1) E_2 + (d_3 - d_2) E_3 + (1 - d_3) E_4 \\ d_1 F_1 + (d_2 - d_1) F_2 + (d_3 - d_2) F_3 + (1 - d_3) F_4 \end{bmatrix} \quad (3)$$

$$x(t) = X + \hat{x}, \quad u(t) = U + \hat{u}, \quad y(t) = Y + \hat{y}, \quad d_1 = D_1 + \hat{d}_1, \\ d_2 = D_2 + \hat{d}_2, \quad d_3 = D_3 + \hat{d}_3, \quad (1 - d_3) = D_3^1 - \hat{d}_3 \quad (4)$$

$$\begin{bmatrix} \hat{v}_0(s) \\ \hat{i}_{g1}(s) \\ \hat{i}_{g2}(s) \end{bmatrix} = \begin{bmatrix} G_{11}(s) & G_{12}(s) & G_{13}(s) \\ G_{21}(s) & G_{22}(s) & G_{23}(s) \\ G_{31}(s) & G_{32}(s) & G_{33}(s) \end{bmatrix} \begin{bmatrix} \hat{d}_1(s) \\ \hat{d}_2(s) \\ \hat{d}_3(s) \end{bmatrix} \quad (5)$$

$$G = \begin{bmatrix} G_{11}(s) & G_{12}(s) & G_{13}(s) \\ G_{21}(s) & G_{22}(s) & G_{23}(s) \\ G_{31}(s) & G_{32}(s) & G_{33}(s) \end{bmatrix} \quad (6)$$

3 Decentralised Controller Structure

Using the TFM G given in Appendix Eq. (A1)-(A9), identify the input-output pairing. It describes which input controls which output predominantly than others. The pairing problem is addressed by performing Interaction Analysis using RGA as given in [24]. The TIID converter's computed matrix is provided in (7). TFM is diagonally dominating, as can be seen from this matrix (0.9505, 0.8920, and 0.9059). As a result, RGA recommends matching the input-output variables of the TIID converter diagonally i.e., $d_1 - V_o$, $d_2 - i_{g1}$ and $d_3 - i_{g2}$. This leads to the decentralized or diagonal controller topology seen in Figure 3.

$$RGA(G(s)) = \begin{bmatrix} 0.9505 & 0.0139 & 0.0356 \\ 0.0495 & 0.8920 & 0.0585 \\ 0.0000 & 0.0941 & 0.9059 \end{bmatrix} \quad (7)$$

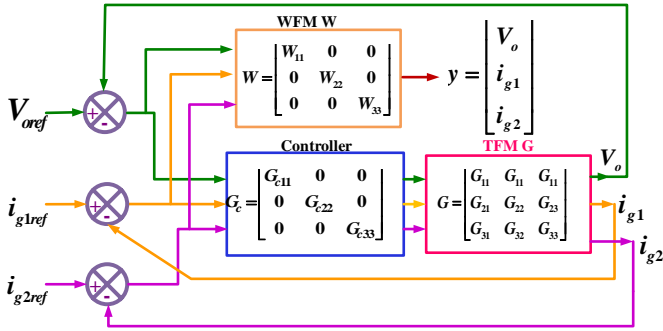


Fig. 3: Schematic of the TIID converter's closed-loop system

The controller G_c is said to be the robust if it rejects disturbances and noises injected at the plant output. The robustness is acquired by direct loop shaping of singular value plots of a closed loop system. The system performance and robustness are described in terms of sensitivities: Sensitivity (S) and complementary sensitivity (T) and controller sensitivity (KS). The required performance objectives of system (S , KS and T) are represented with weight functions (loop-shaping filters) W_1 , W_2 and W_3 respectively. These are incorporated into the system before designing the controller G_c . Weight Function Matrix (WFM) (loop-shaping filters) is given in (8) and is designed using the principles given in [25]. WFM is the frequency dependent and represents the frequency response upper bound of the S , KS , and T .

$$W(s) = \begin{bmatrix} W_1 S \\ W_2 KS \\ W_3 T \end{bmatrix} \quad (8)$$

4 CRCBP Controller For TIID Converter

For the TIID converter, any deviation in line voltages V_{g1} , V_{g2} , V_{g3} and load will reflect in converter dynamics and its characteristics. A robust controller is required to govern the three output variables of the TIID converter to handle this unpredictable scenario. is considered resilient when there is uncertainty present but the closed-loop system remains stable, [26]. As was previously mentioned, the WFM is used to indicate the controller's performance and resilience. In the CRCBP method, RPM $\Gamma(\omega)$ is defined based on the mixed sensitivity- H_∞ control of WFM i.e.,

$\Gamma(\omega)$ is the maximum singular value ($\bar{\sigma}$) of WFM as given in (9). In this method, the sufficient condition for a closed-loop converter system to be robust is the RPM $\Gamma(\omega) < 1 \forall \omega$.

$$\Gamma(\omega) = \bar{\sigma}(W(s)) = \bar{\sigma} \left(\begin{bmatrix} W_1 S \\ W_2 KS \\ W_3 T \end{bmatrix} \right) \quad (9)$$

The CRCBP are contours of RPM $\Gamma(\omega)$, which are set over the controller's bode magnitude and phase charts. The contours of RPM where $\Gamma(\omega) \geq 1$ are termed as forbidden regions. The controller is not robust in the frequency range if the controller frequency response crosses these contours. Thus, the objective is to choose the controller G_c iteratively, such that its frequency response doesn't intersect with the forbidden regions at all frequencies. As a result, the CRCBP approach makes it easier to optimize the controller iteratively since the plots make it evident where the RPM contours are in relation to the prohibited regions. Additionally, this method allows for flexibility in choosing the controller parameters without changing the weighting functions. This approach works better with converters that have fluctuating operating points and unclear parameters.

4.1 Implementation of CRCBP Controller for TIID converter

In this section, the procedure to tune the PI controller parameters of G_{c1} to control G_{11} of TIID converter using CRCBP is presented and these are iteratively obtained in MATLAB environment. In each iteration, the bode plots of the controller are observed so as not to intersect with forbidden regions of RPM $\Gamma(\omega) \geq 1$. If the intersections are found, then the controller is not robust so the iterations are repeated till a robust controller is obtained. Before designing G_{c1} , the WFM is to be constructed first. W_1 and W_3 are selected as given in (10). The controller effort is not limited so $W_2 = 0$.

$$W_1 = \frac{s+20}{2s+1} \quad W_2 = 0 \quad W_3 = \frac{s+500}{0.005s+1000} \quad (10)$$

4.1.1 Iteration 1

Choose G_{c1} as a Proportional Controller ($K_p = 1$). Figure 4 displays the CRCB charts for the closed loop system. The area of G_{c1} where the forbidden region intersects is indicated by the red part ($\Gamma(\omega) \geq 1$), implying that the designed controller is not robust. Figure 5 shows the Bode Magnitude Frequency Response (BMFR) of $1/W_1$, S_1 and $1/W_3, T_1$ and indicates that $1/W_3$ is below T_1 in high frequency region. Thus, closed-loop complementary sensitivity function is violating the constraint in the high frequency region indicating that the system is exhibiting poor disturbance rejection characteristics which caused the interaction with the forbidden region in high frequency region as shown in Figure 4. So, the controller needs to have integral action to compensate this.

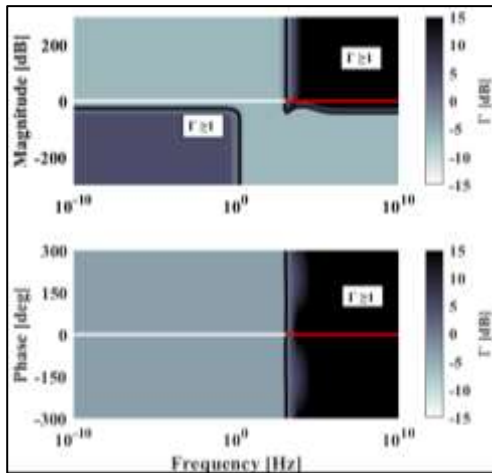


Fig. 4: CRCBP of G_{c1} and G_{11}

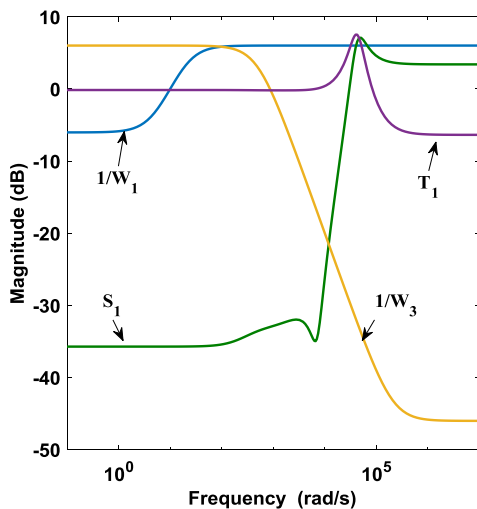


Fig. 5: BMFR of $1/W_1$, S_1 and $1/W_3, T_1$

4.1.2 Iteration 2

Choose G_{c1} as a combination of Proportional and Integral Controller ($K_p = 1, K_I = 1$). The CRCB plots of the closed loop system are plotted in Figure 6. The BMFR of $1/W_1$, S_1 and $1/W_3, T_1$ is shown in Figure 7. The Figures are identical to that in iteration 1. So, the controller parameters are to be adjusted further.

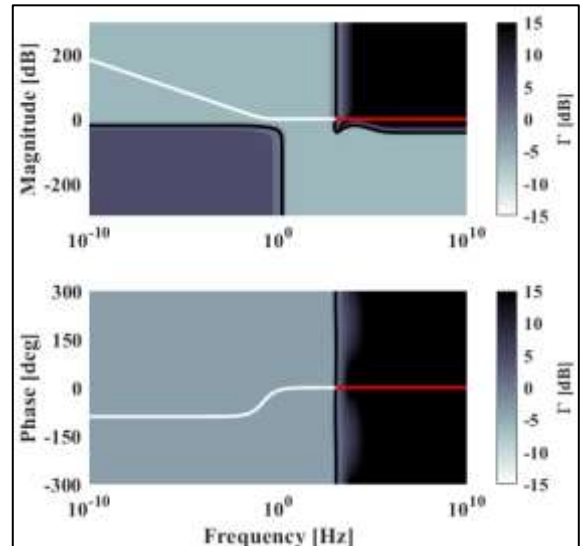


Fig. 6: CRCBP of G_{c11} and G_{11}

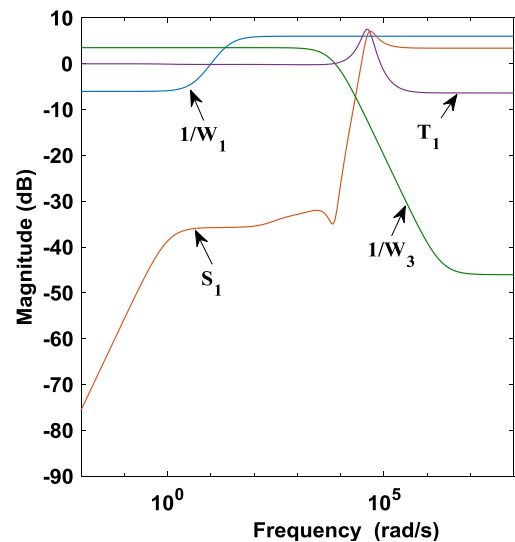


Fig. 7: BMFR of $1/W_1$, S_1 and $1/W_3, T_1$

4.1.3 Iteration 3

G_{c1} is taken as solely Integral Controller ($K_I = 0.95$). The CRCB plots and BMFR are shown in Figure 8 and Figure 9 respectively and show that there are no interactions with the forbidden region implying the robustness of the

controller. Figure 9 shows that $1/W_1$ and $1/W_3$ satisfy the upper bounds of S_1 and T_1 .

$$G_{c3} = \frac{0.0052s + 1.05}{s} \quad (12)$$

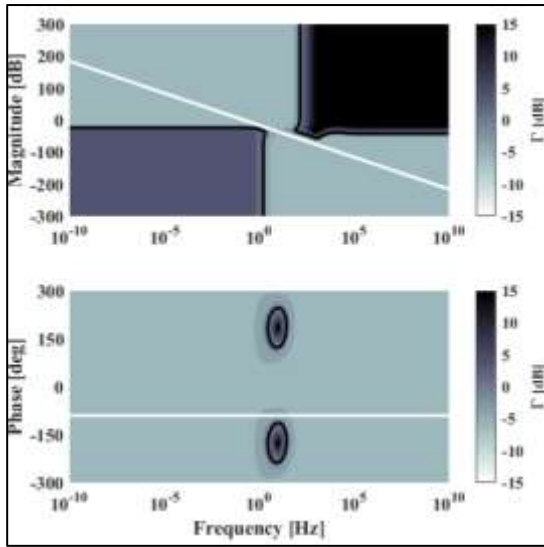


Fig. 8: CRCBP of G_{c11} and G_{11}

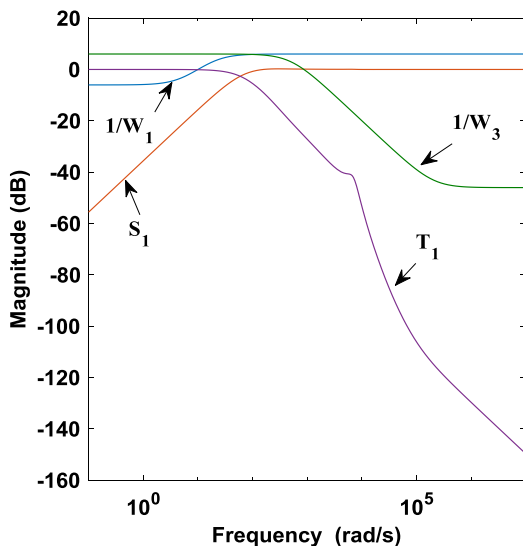


Fig. 9: BMFR of $1/W_1$, S_1 and $1/W_3$, T_1

Similarly, G_{c2} and G_{c3} are designed and are given below in Eqs. (11) and (12). The CRCBP plots are shown in Figure 10 and Figure 11 respectively. The corresponding BMFR plots are shown in Figure 12 and Figure 13. These plots show that the $1/W_1$ and $1/W_3$ satisfy the upper bounds of S_2 , T_2 and S_3 , T_3 respectively.

$$G_{c2} = \frac{0.03s + 2.9171}{s} \quad (11)$$

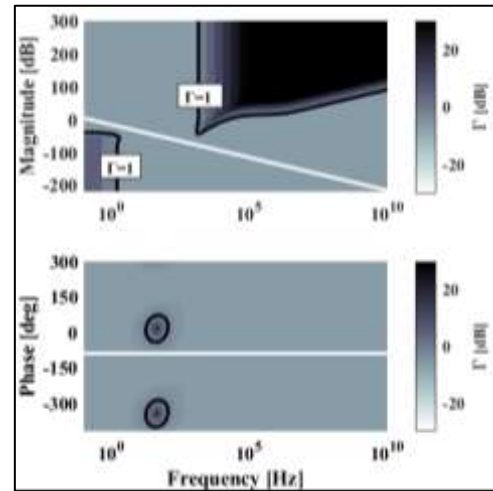


Fig. 10: CRCBP of G_{c2} and G_{22}

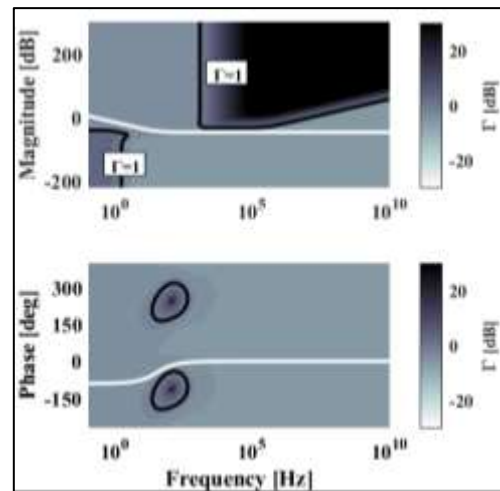


Fig. 11: CRCBP of G_{c3} and G_{33}

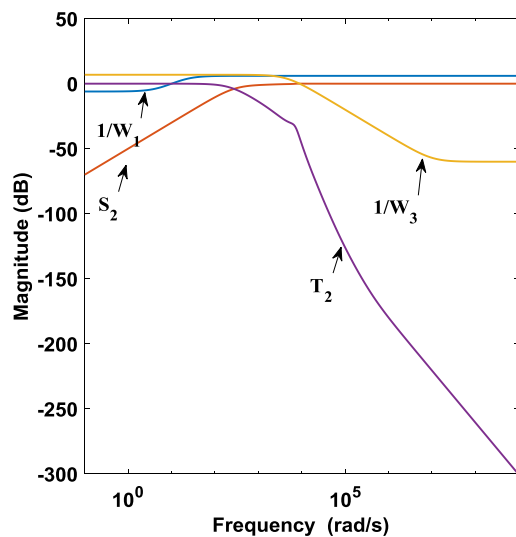


Fig. 12: BMFR of $1/W_1$, S_2 and $1/W_3$, T_2

5 Results and Discussions

The test bench is shown in Figure 14, and MATLAB connected with the OPAL4510-RT simulator using RT-LAB simulation software confirms the closed-loop performance of G_c for TIID converter. The Hardware-in-the-Loop (HIL) testing apparatus is called OPAL4510-RT, [27], [28]. This is used to simulate the converter, and real-time observations are made using an oscilloscope for digital storage. Under various operating scenarios, the robust controller's performance is validated.

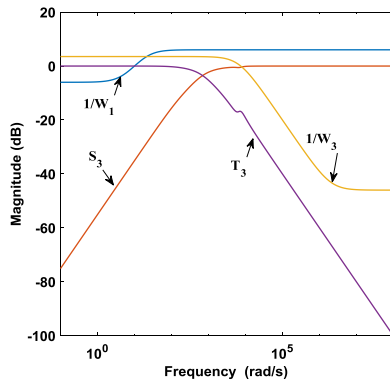


Fig. 13: BMFR of $1/W_1$, S_3 and $1/W_3$, T_3



Fig. 14: OPAL4510-RT Simulator test bench

Figure 15 displays the simulation findings that match the nominal settings given in Table A1 (Appendix) and Figure 16 displays the HIL Simulation results of the OP4510 measured in DSO.

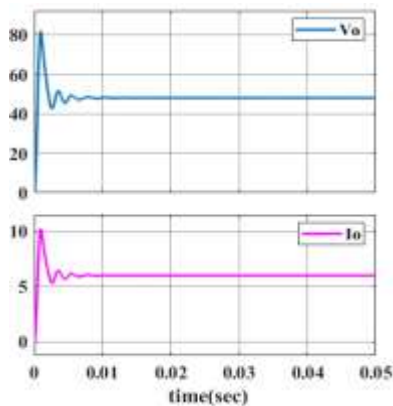


Fig. 15: V_o , I_o of TIID converter

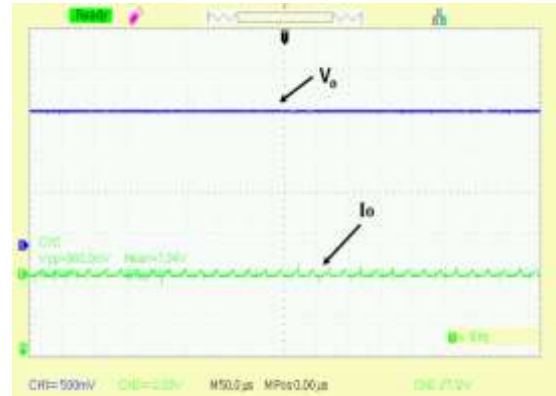


Fig. 16: V_o , I_o of TIID converter

5.1 Case I: Under Varying Load Conditions

In this case, R_o is varied from 8Ω to 10Ω at $t=25\text{msec}$ and from 10Ω to 12Ω at $t=60\text{msec}$ and again reduced from 12Ω to 8Ω at $t=80\text{msec}$. The simulation results of the corresponding output voltage V_o and the load currents I_o are given in Figure 17. It is observed from this Figure, that when R_o is increased at $t=25\text{msec}$, V_o is regulated by d_1 and I_o is reduced with increase in R_o . Similarly, at $t=60\text{msec}$ and at $t=80\text{msec}$, V_o is regulated by d_1 and I_o varies with the variation in R_o . Hence, the designed controller is able to regulate V_o at the desired value of 48V with variations of load conditions.

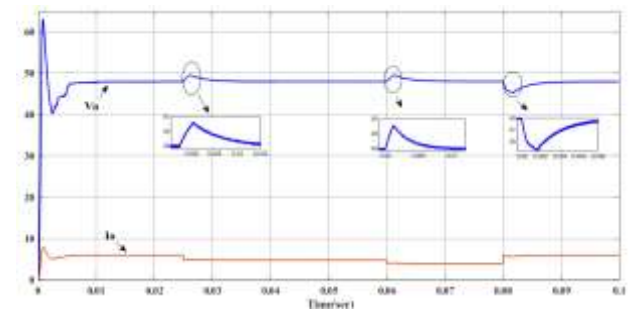


Fig. 17: V_o , I_o of TIID converter under varying load conditions

5.2 Case II: Under Varying Source Voltages

In this case, the source voltages are varied at different times individually keeping the other sources at nominal values, and the corresponding V_o and I_o are observed. At $t=40\text{msec}$, the input voltage V_{g3} is varied from 24V to 20V keeping the other two sources V_{g1} and V_{g2} at nominal values.

At $t=60\text{msec}$, V_{g2} is varied from 30V to 25V with V_{g1} and V_{g3} at nominal values. At $t=80\text{msec}$, V_{g1} is varied from 36V to 30V with V_{g2} and V_{g3} at nominal values. The simulation results of the corresponding V_o and I_o are given in Figure 18.

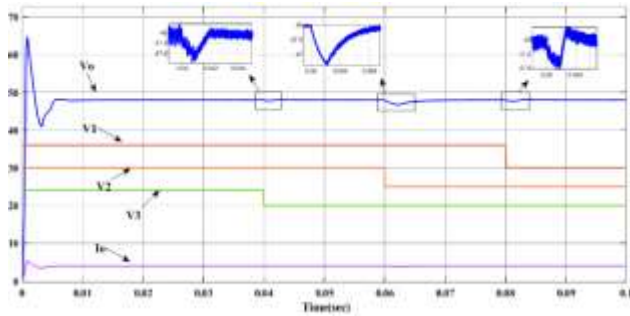


Fig 18: V_o , I_o of TIID converter with varying source voltages

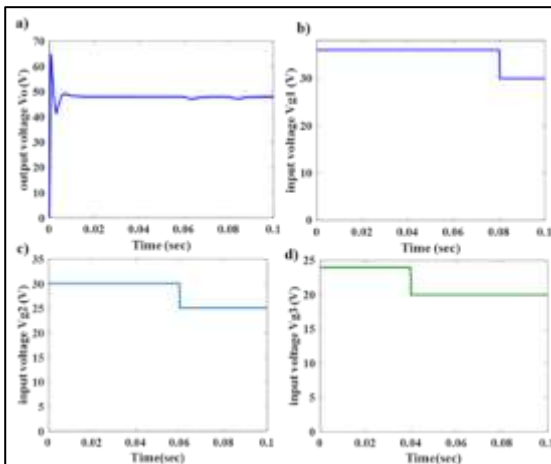


Fig. 19: a) V_o from DLM, b) V_{g1} from DLM, c) V_{g2} from DLM, d) V_{g3} from DLM

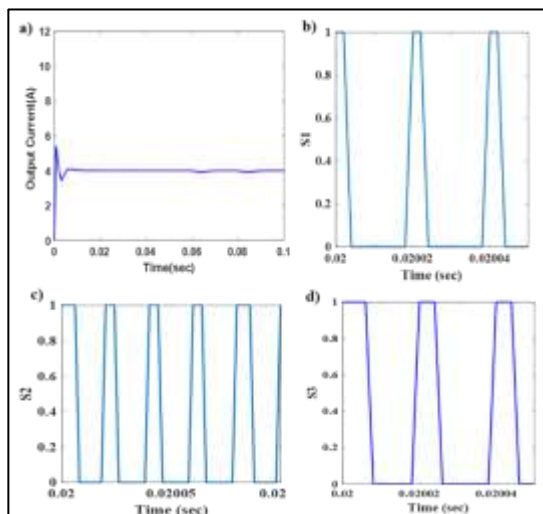


Fig. 20. a) I_o from DLM, b) d_1 of switch S_1 , c) d_2 of S_2 d) d_3 of S_3 from DLM

The HIL simulation results using the Data Logger Method (DLM) are given from Figure 19 (a)-(d) and Figure 20 (a)-(d). The HIL simulation results measured in CRO are given in Figure 21, Figure 22, Figure 23, Figure 24 and Figure 25.

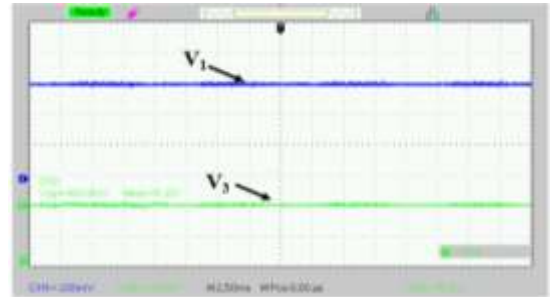


Fig. 21: Input voltage V_{g1} and V_{g3} of TIID converter

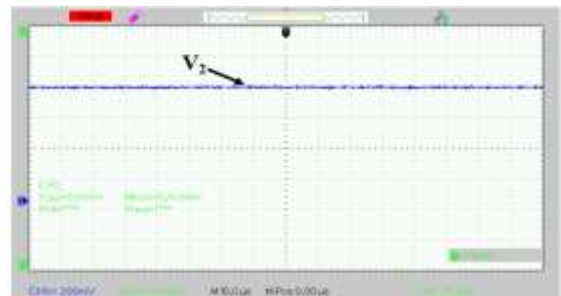


Fig. 22: Input voltage V_{g2} of TIID converter

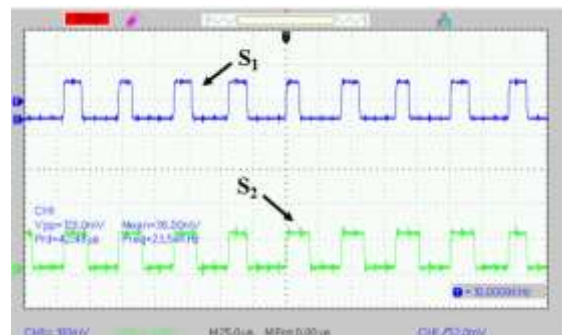


Fig. 23: Duty ratios of S_1 and S_2 of TIID converter

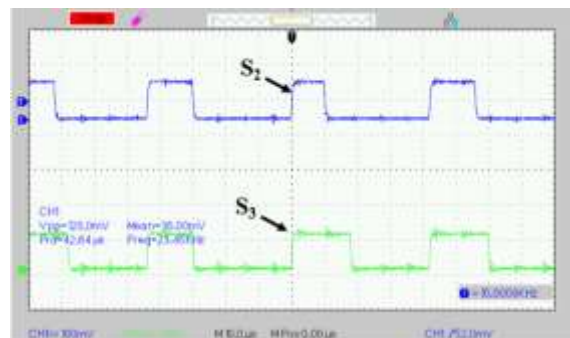


Fig. 24: Duty ratios of S_2 and S_3 of TIID converter

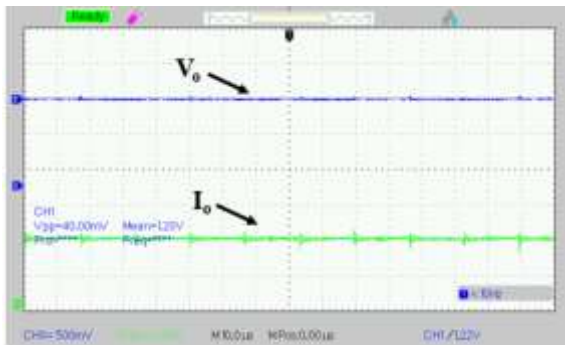


Fig. 25: V_o , I_o of TIID converter

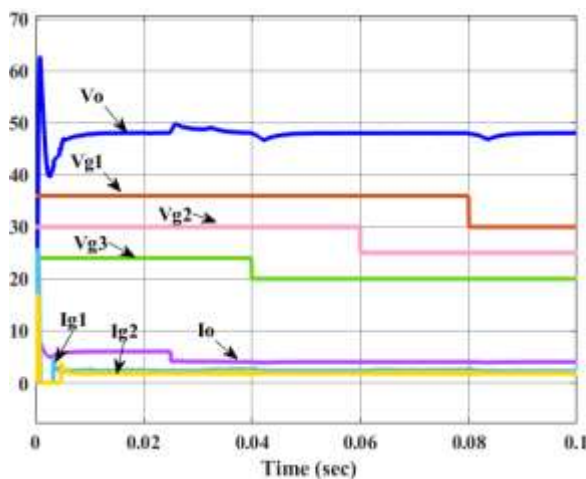


Fig. 26: V_o , I_o of TIID converter in case (iii)

5.3 Case III: Under Both Load and Sources are Varying:

In this case, the load and the source voltages are varied and the corresponding V_o and I_o are observed. R_o is varied from 8Ω to 12Ω at $t=25\text{msec}$, at $t=40\text{msec}$, V_{g3} is varied from 24V to 20V, at $t=60\text{msec}$, V_{g2} is varied from 30V to 25V and at $t=80\text{msec}$, V_{g1} is varied from 36V to 30V. The simulation results of the corresponding V_o and I_o are given in Figure 26.

5.4 Comparison with SISO PID TUNER

The obtained CRCBP controller performance is compared with SISO tuned PID controller, [5]. The time domain parameters of the two controllers for the system G_{11} are compared and shown in Table 1, it is evident that the CRCBP controller outperformed the PI controller in terms of performance. Figure 27 (Appendix) presents a comparison of the closed-loop performances of the PI and CRCBP controllers under various settings,

including variations in both input voltages and load (as in case iii).

Both controllers can maintain an output voltage of 48V under a variety of circumstances but, the CRCBP controller is able to regulate swiftly in terms of all the time-domain characteristics as shown in Table 1.

Table 1. Comparison of PI and CRCBP controller performance of G_{11} system.

| Controller for G_{11} | PI | CRCBP |
|-------------------------|----------|----------|
| Rise Time | 8.1 msec | 2.8 msec |
| Transient Time | 12 msec | 5.3 msec |
| Settling Time | 12 msec | 5.3 msec |
| Overshoot | 1.2591 | 0 |
| Undershoot | 0 | 0.0224 |
| Peak | 1.0126 | 0.9658 |
| Peak Time | 0.0179 | 0.0100 |

6 Conclusion

A robust PID controller based on the Contoured Robust Controller Bode Plot (CRCBP) is designed for control of the three-input integrated Dc-Dc (TIID) converter. The TIID converter is modeled using state-space analysis and a Transfer Function Matrix (TFM) is acquired from the small signal continuous time model. Further, the weight functions (loop-shaping filters) are designed based on the TFM which represents the desired robustness and performance of the controller. A conventional TIID converter with a power rating of 288 W and input voltage levels of 24 V, 30 V, and 36 V is taken into consideration to demonstrate how well the suggested controller works in different working environments. The Hardware-in-Loop (HIL) results are obtained with MATLAB integrated OPAL RT simulator OP4510.

The Future scope of this research work is (i) to design a DC Microgrid with three different Renewable energy sources that uses the proposed TIID converter, (ii) to regulate the output voltage of a DC Microgrid with PI controllers, that are to be designed by CRCBP method, (iii) the relation between RPM and Sensitivity at different stages of controller design are to be graphically studied and (iv) the violation of sensitivity and RPM plots at each iteration are to be addressed.

References

- [1] X. L. Li, Z. Dong, C. K. Tse and D. D. -C. Lu, "Single-Inductor Multi-Input Multi-Output DC-DC Converter With High Flexibility and

- Simple Control," in *IEEE Transactions on Power Electronics*, vol. 35, no. 12, pp. 13104-13114, Dec. 2020.
- [2] Deepak Agrawal, Rajneesh Kumar Karn, Deepak Verma, Rakeshwri Agrawal, "Modelling and Simulation of Integrated Topology of DC/DC converter for LED Driver Circuit," *WSEAS Transactions on Electronics*, vol. 11, pp. 18-21, 2020, <https://doi.org/10.37394/232017.2020.11.3>.
- [3] H. Matsuo, W. Lin, F. Kurokawa, T. Shigemizu, and N. Watanabe, "Characteristics of the multiple-input dc-dc converter," *IEEE Transactions on Industrial Electronics*, vol. 51, no. 3, pp. 625-631, Jun. 2004.
- [4] A. Gupta, R. Ayyanar and S. Chakraborty, "Novel Electric Vehicle Traction Architecture With 48 V Battery and Multi-Input, High Conversion Ratio Converter for High and Variable DC-Link Voltage," in *IEEE Open Journal of Vehicular Technology*, vol. 2, pp. 448-470, 2021.
- [5] I. Alhamrouni, M. Salem, Y. Zahraoui, B. Ismail, A. Jusoh, and T. Sutikno, "Multi-input interleaved DC-DC converter for hybrid renewable energy applications," *Bulletin of Electrical Engineering and Informatics*, vol. 11, no. 3, pp. 1765-1778, Jun. 2022.
- [6] B. R. Ravada, N. R. Tummuru and B. N. L. Ande, "Photovoltaic-Wind and Hybrid Energy Storage Integrated Multi-Source Converter Configuration for DC Microgrid Applications," in *IEEE Transactions on Sustainable Energy*, vol. 12, no. 1, pp. 83-91, Jan. 2021.
- [7] E. Amiri, R. R. Khorasani, E. Adib and A. Khoshkbar-Sadigh, "Multi-Input High Step-Up DC-DC Converter With Independent Control of Voltage and Power for Hybrid Renewable Energy Systems," in *IEEE Transactions on Industrial Electronics*, vol. 68, no. 12, pp. 12079-12087, Dec. 2021, doi: 10.1109/TIE.2020.3047038.
- [8] T. H. K. J. Åström, *Advanced PID control*. Instrumentation, Systems, and Automation Society Research Triangle Park, NC, 2006.
- [9] B. A. Reddy and M. Veerachary, "Gramian based digital controller design for two-input integrated DC-DC converter," 2013, [Online]. <https://ieeexplore.ieee.org/document/6731675> (Accessed Date: September 07, 2023).
- [10] Dahale, Shweta & Das, Aakriti & Pindoriya, Naran & Rajendran, S.. (2017). An overview of DC-DC converter topologies and controls in DC microgrid. 410-415. <https://doi.org/10.1109/ICPES.2017.8387329>.
- [11] M. Veerachary, "Two-loop controlled buck-SEPIC converter for input source power management," *IEEE Transactions on Industrial Electronics*, vol. 59, no. 11, pp. 4075-4087, Nov, 2012, <http://doi.org/10.1109/TIE.2011.2174530>.
- [12] Michael. Green and D. J. N. Limebeer, "Linear robust control", Prentice Hall, 1995.
- [13] Kubo, Takayuki & Yubai, Kazuhiro & Yashiro, Daisuke & Hirai, Junji. (2015). Weight optimization for H_∞ loop shaping method using frequency response data for SISO stable plant. Proceedings - 2015 *IEEE International Conference on Mechatronics, ICM* 2015. 246-251, <https://doi.org/10.1109/ICMECH.2015.7083982>.
- [14] Q. Xiong and W. J. Cai, "Effective transfer function method for decentralized control system design of multi-input multi-output processes," *J Process Control*, vol. 16, no. 8, pp. 773-784, Sep. 2006, <https://doi.org/10.1016/j.procon.2006.04.001>.
- [15] W. E. Leithead and J. O'Reilly, "Multivariable control by individual channel design: an automotive gas turbine case study," *International Conference on Control 1991. Control '91*, Edinburgh, UK, 1991, pp. 1261-1266, vol.2.
- [16] G. Willmann, D. F. Coutinho, L. F. A. Pereira, and F. B. Libano, "Multiple-Loop H-Infinity Control Design for Uninterruptible Power Supplies," *IEEE Transactions on Industrial Electronics*, vol. 54, no. 3, pp. 1591-1602, Jun. 2007, <https://doi.org/10.1109/TIE.2007.894721>.
- [17] P. Apkarian and D. Noll, "The H_∞ Control Problem is Solved", <http://doi.org/10.12762/2017.AL13-01>.
- [18] P. Nordfeldt and T. Hägglund, "Decoupler and PID controller design of TITO systems," *J Process Control*, vol. 16, no. 9, pp. 923-936, Oct. 2006, <https://doi.org/10.1016/j.procon.2006.06.002>.
- [19] J. D. Taylor and W. Messner, "Controller Design for Nonlinear Multi-Input/Multi-Output Systems Using The Contoured Robust Controller Bode Plot" *International Journal Of Robust And Nonlinear Control*, vol. 24, no. 18, pp. 3196-3213, 2013.
- [20] Xia, Lu and William C. Messner. "Loop shaping for robust performance using Rbode plot." *Proceedings of the 2005, American*

Control Conference, 2005. (2005): 2869-2874 vol. 4.

- [21] M. Veerachary and P. Shaw, "Controller Design and Analysis for Fifth-Order Boost Converter," *IEEE Trans Ind Appl*, vol. 54, no. 5, pp. 4894–4907, Sep. 2018.
- [22] M. Manogna, A. B. Amarendra Reddy, and K. Padma, "Modeling of a Three-Input Fourth-Order Integrated DC-DC Converter," in *Proceedings - 2022 International Conference on Smart and Sustainable Technologies in Energy and Power Sectors, SSTEPS 2022*, Institute of Electrical and Electronics Engineers Inc., 2022, pp. 83–88. <https://doi.org/10.1109/SSTEPS57475.2022.00032>.
- [23] Y. C. Liu and Y. M. Chen, "A systematic approach to synthesizing multi-input DC-DC converters," *IEEE Trans Power Electron*, vol. 24, no. 1, pp. 116–127, 2009, <https://doi.org/10.1109/TPEL.2008.2009170>.
- [24] M. Manogna, B. A. Reddy, and K. Padma, "Interaction measures in a three-input integrated DC-DC converter," *Engineering Research Express*, vol. 5, no. 1, Mar. 2023, <https://doi.org/10.1088/2631-8695/acc0dc>.
- [25] K. and J. C. Doyle. Zhou, *Essentials of Robust Control*. Upper Saddle River, Prentice-Hall, 1999, ISBN: 978-0135258330.
- [26] S. Skogestad and I. Postlethwaite, *Multivariable Feedback Control: Analysis and Design*. New York, NY, USA: Wiley, 2005. 2001.
- [27] A. A. Bhandakkar and L. Mathew, "Real-Time-Simulation of IEEE-5-Bus Network on OPAL-RT-OP4510 Simulator," in *IOP Conference Series: Materials Science and Engineering*, Institute of Physics Publishing, Mar. 2018, <http://doi.org/10.1088/1757-899X/331/1/012028>.
- [28] A. D. Roy and C. Umayal, "Opal-rt based analysis and implementation of single phase cascaded multilevel inverter with minimum number of switches," *Indian J Sci Technol*, vol. 9, Special Issue 1, Dec 2016, [https://doi.org/10.17485/ijst/2016/v9iS\(1\)97744](https://doi.org/10.17485/ijst/2016/v9iS(1)97744).

Contribution of Individual Authors to the Creation of a Scientific Article (Ghostwriting Policy)

The authors equally contributed in the present research, at all stages from the formulation of the problem to the final findings and solution.

Sources of Funding for Research Presented in a Scientific Article or Scientific Article Itself

No funding was received for conducting this study.

Conflict of Interest

The authors have no conflicts of interest to declare.

Creative Commons Attribution License 4.0 (Attribution 4.0 International, CC BY 4.0)

This article is published under the terms of the Creative Commons Attribution License 4.0

https://creativecommons.org/licenses/by/4.0/deed.en_US

APPENDIX

The TIID converter operates on a 48V dc-bus regulation. Table A1 lists the specifications that are taken into consideration here. With these parameters, MATLAB calculates the TFM G of the TIID converter taking into account every mode described in section 2 and provides G as given in (5) from (A1)- (A9).

Table A1. Specifications and Parameter Values

| Parameters | Value |
|-------------------------------|-------------------------------------|
| V_{g1}, V_{g2}, V_{g3} | 36V,30V,24V |
| $V_o, \text{Load power } P_o$ | 48V, 288W |
| i_{L1}, i_{L2} | 2.5A,2A |
| L_1, L_2, L_3 | 150 μ H,250 μ H, 20 μ H |
| C_o | 200 μ F |
| Switching frequency f_s | 50KHz |
| $\Delta i_L, \Delta V_o$ | 10%, 5% |

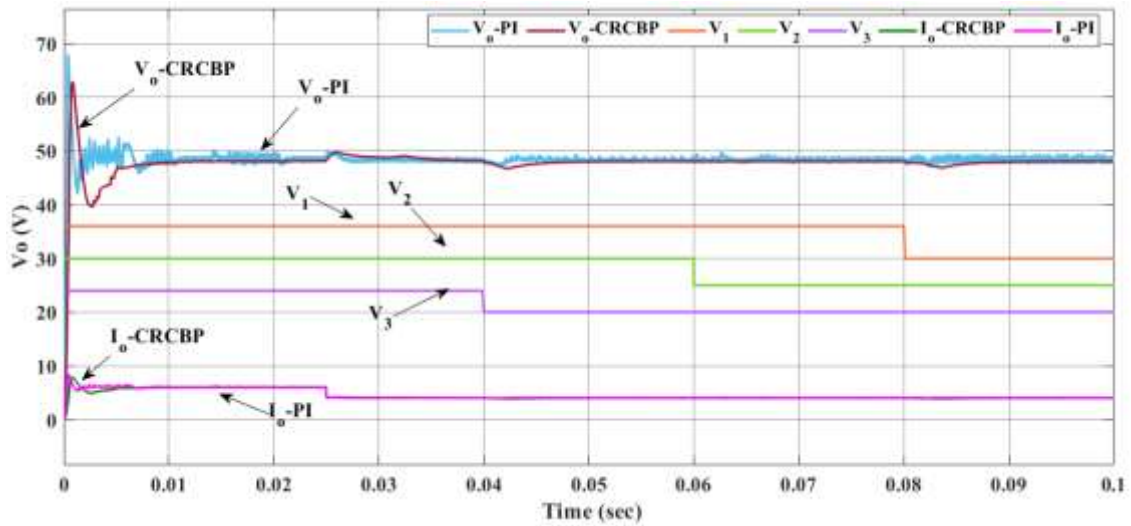


Fig. 27: V_o, I_o of TIID converter with CRCBP and PI under varying conditions

$$G_{11} = \frac{-0.3488s^4 - 2.493x10^4 s^3 + 1.051x10^9 s^2 + 5.608x10^{12} s + 1.796x10^{15}}{s^4 + 6195s^3 + 6.126x10^7 s^2 + 1.3x10^{11} s + 2.885x10^{13}} \quad (A1)$$

$$G_{12} = \frac{0.6379s^4 + 1.293x10^5 s^3 + 6.573x10^9 s^2 + 2.308x10^{12} s + 6.963x10^{13}}{s^4 + 6195s^3 + 6.126x10^7 s^2 + 1.3x10^{11} s + 2.885x10^{13}} \quad (A2)$$

$$G_{13} = \frac{-0.4423s^4 - 4.073x10^4 s^3 + 3.755x10^8 s^2 + 2.48x10^{12} s + 8.226x10^{13}}{s^4 + 6195s^3 + 6.126x10^7 s^2 + 1.3x10^{11} s + 2.885x10^{13}} \quad (A3)$$

$$G_{21} = \frac{3.249x10^5 s^3 + 2.093x10^9 s^2 + 1.442x10^{13} s + 1.382x10^{16}}{s^4 + 6195s^3 + 6.126x10^7 s^2 + 1.3x10^{11} s + 2.885x10^{13}} \quad (A4)$$

$$G_{22} = \frac{-4253s^3 - 7.506x10^8 s^2 - 3.238x10^{13} s - 1.029x10^{16}}{s^4 + 6195s^3 + 6.126x10^7 s^2 + 1.3x10^{11} s + 2.885x10^{13}} \quad (A5)$$

$$G_{23} = \frac{2949s^3 + 1.943 \times 10^8 s^2 - 1.899 \times 10^{12} s - 1.215 \times 10^{16}}{s^4 + 6195s^3 + 6.126 \times 10^7 s^2 + 1.3 \times 10^{11} s + 2.885 \times 10^{13}} \quad (A6)$$

$$G_{31} = \frac{4.446 \times 10^7 s^2 - 2.665 \times 10^{12} s - 1.243 \times 10^{16}}{s^4 + 6195s^3 + 6.126 \times 10^7 s^2 + 1.3 \times 10^{11} s + 2.885 \times 10^{13}} \quad (A7)$$

$$G_{32} = \frac{-2552s^3 - 4.15 \times 10^8 s^2 - 1.577 \times 10^{13} s - 1.4 \times 10^{15}}{s^4 + 6195s^3 + 6.126 \times 10^7 s^2 + 1.3 \times 10^{11} s + 2.885 \times 10^{13}} \quad (A8)$$

$$G_{33} = \frac{1.967 \times 10^5 s^3 + 1.237 \times 10^9 s^2 + 1.061 \times 10^{13} s + 1.592 \times 10^{16}}{s^4 + 6195s^3 + 6.126 \times 10^7 s^2 + 1.3 \times 10^{11} s + 2.885 \times 10^{13}} \quad (A9)$$